optica

Freestyle 3D laser traps: tools for studying light-driven particle dynamics and beyond

José A. Rodrigo* and Tatiana Alieva

Universidad Complutense de Madrid, Facultad de Ciencias Físicas, Ciudad Universitaria s/n, Madrid 28040, Spain
**Corresponding author: jarmar@fis.ucm.es*

Received 11 May 2015; revised 22 July 2015; accepted 19 August 2015 (Doc. ID 240710); published 14 September 2015

We show that a freestyle laser trap, including high-intensity and phase gradient forces along arbitrary curves, is able to confine multiple particles and drive their motion with the ability to speed them up or slow them down. This Letter reports, for first time, to the best of our knowledge, how such a trap can be experimentally created deep within the sample to construct rotating colloidal motors and study collective particle dynamics in distinct configurations. This new laser tool opens up promising perspectives in the study of hydrodynamics and optofluidics at the microscale.

OCIS codes: (140.3300) Laser beam shaping; (140.7010) Laser trapping; (170.4520) Optical confinement and manipulation.

http://dx.doi.org/10.1364/OPTICA.2.000812

Numerous applications in microscience, nanoscience, and technology require trapping and manipulation of dielectric colloidal particles. The controlled motion of these particles induces fluid flows suited for the study of hydrodynamical microsystems and microrheology. For instance, rotating colloidal motors of dielectric particles can be used for local mixing in microfluidics and for analysis of hydrodynamic interactions between microscopic objects and complex microsystems, such as Brownian ratchets [1–3]. During the past few decades, optical traps, created by focusing a laser beam with a high-numerical-aperture (NA > 1) microscope objective lens, have been demonstrated to be an essential tool for these applications [4]. The use of digital holography techniques for laser beam shaping and particle tracking has revolutionized microscale and nanoscale particle manipulation, force and position measurements. In particular, the holographic generation of laser vortex beams able to exert torque over the trapped particles (see [5–9] and references cited therein) allows creating optically driven micropumps [7–9]. However, a Gaussian vortex trap in a ring-like or other shape [6] has important limitations due to its weak axial intensity gradient, which is unable to compensate the light scattering force. This fact explains why Gaussian vortex traps confine only the particles pushed against the coverslip glass that acts the sample's chamber or another media interface (e.g., water–air [8]). Three-dimensional (3D) multiparticle manipulation can also be performed by using fast temporal control of multiple spot-like traps generated by computer-generated holograms [10,11]. This approach is well suited for assembly of structures and individual particle control but not for study of multiparticle dynamics. Moreover, it requires high-speed computation and spatial light modulators (SLMs). Other proposals for transport of multiple particles exploit specific characteristics of Bessel [12] and Airy [13] beams, but the achieved particle trajectories are fixed.

A *true* 3D vortex trap able to confine one or multiple particles without the help of the chamber walls and move them around a ring [14] has been created using a focused helical Bessel beam. Specifically, in contrast to a Gaussian vortex, the high-intensity gradients (HIGs) of this beam allow for 3D trapping, while the phase gradient force created by the vortex drives the particle motion along the ring [14,15]. The HIGs and phase gradient forces [15] are crucial for the construction of 3D laser traps that are able to move multiple particles even against light radiation pressure [16,17]. This is a key point in the design of 3D curved traps [17–19], where in some regions the directions of beam propagation and particle motion are opposite. Moreover, in the mentioned applications, particles with a size typically in the range of 200–1000 nm have to be trapped deep within the sample, far enough from the chamber walls to avoid unwanted hydrodynamic perturbations due to proximal wall effects. This is particularly difficult to achieve because stable trapping with a high NA lens is often limited to a few micrometers from the bottom surface of the chamber [20,21]. Another challenging problem is the creation of single-beam freestyle traps—whose form and driving forces can be adapted to specific tasks—able to move in 3D such small particles in a controlled way. Their HIGs and phase gradients have to be independently prescribed along the curve in order to speed up or slow down the particle motion without changing the trap shape and size.

In this Letter we demonstrate how, using the holographic technique developed in [19] for 3D beam shaping, to create freestyle traps that satisfy the above-listed requirements. We experimentally validate the capability of these traps—in the form of ring, triangle, square, and 3D curves including a toroidal-spiral one—for motion control of 1 μm dielectric particles up to 25 μm deep within the sample. These particles are small enough to predict the trapping of nanoparticles and large enough to track them and characterize their flow in the 3D trap. We have found that freestyle traps with geometries different from the ring have an

intrinsic inhomogeneous phase distribution that explains the observed nonuniform particle motion. This fact and the straightforward design of the freestyle trap open up new routes for the study of collective particle dynamics.

Our trapping setup comprises an inverted microscope, a standard reflective SLM (Holoeye PLUTO, pixel size of 8 μm), and a high speed sCMOS camera (Hamamatsu, Orca Flash 4.0, 16-bit gray-level, pixel size of 6.5 μm). To generate the trapping beam, a phase-only hologram addressed into the SLM modulates an input collimated laser beam (Laser Quantum, Ventus, $\lambda = 532$ nm, 1.2 W), which is then projected (with a 1× Keplerian telescope) into the back aperture of the microscope objective lens (Olympus UPLSAPO, 1.4 NA, 100×, oil immersion), as reported in [19]. Finally, this lens highly focuses the latter beam (power of 170 mW at lens input) generating the 3D trap in a sample that includes 1 μm silica particles (Bang Labs) dispersed in deionized water. The sample is enclosed in a chamber made by attaching a glass coverslip (thickness 0.17 mm) to a standard microscope slide. To reach the ability of trapping deep within the sample, an immersion oil with higher refractive index ($n = 1.56$, Cargille Labs, Series A) than the standard one ($n = 1.51$) is used; see [20,21]. By using this kind of immersion oil, the trap stiffness can be increased by up to a factor 3 to stably trap 1 μm dielectric particles up to 50 μm deep in the sample, as reported in [21].

The freestyle trap, in the form of a 3D curve $\mathbf{c}_3(t)$, is generated by using the holographic beam-shaping technique reported in [19]. It consists in the encoding of the complex function

$$H(\mathbf{r}|\mathbf{c}_3(t), t \in [0, T]) = \frac{1}{L}\int_0^T \Phi(\mathbf{r}, t)\varphi(\mathbf{r}, t)|\mathbf{c}_2'(t)|\mathrm{d}t \qquad (1)$$

as a hologram into the SLM. In Eq. (1), $\mathbf{r} = (x, y)$, $\mathbf{c}_3(t) = (x_0(t), y_0(t), z_0(t))$ is the parametrized 3D curve whose projection in the x–y plane is $\mathbf{c}_2(t) = (x_0(t), y_0(t))$. Here, $L = \int_0^T |\mathbf{c}_2'(t)|\mathrm{d}t$ is a length where $|\mathbf{c}_2'(t)| = (x_0'(t)^2 + y_0'(t)^2)^{1/2}$ and $\mathbf{c}_2'(t) = \mathrm{d}\mathbf{c}_2/\mathrm{d}t$. The first term in the integral $H(\mathbf{r}|\mathbf{c}_3)$, which shapes the trapping beam, is given by

$$\Phi(\mathbf{r}, t) = \exp\left(\frac{\mathrm{i}}{\rho^2}[yx_0(t) - xy_0(t)]\right)\exp\left(\frac{\mathrm{i}2\pi m}{S(T)}S(t)\right), \qquad (2)$$

where $S(t) = \int_0^t [x_0(\tau)y_0'(\tau) - y_0(\tau)x_0'(\tau)]\mathrm{d}\tau$, with ρ being a constant and m a free parameter that allows for controlling the phase gradient along the curve. Finally, the term $\Phi(\mathbf{r}, t)$ is modulated in Eq. (1) by the quadratic phase

$$\varphi(\mathbf{r}, t) = \exp\left(\mathrm{i}\pi\frac{[x - x_0(t)]^2 + [y - y_0(t)]^2}{\lambda \mathrm{f}^2}z_0(t)\right), \qquad (3)$$

according to the z coordinate of the prescribed curve $\mathbf{c}_3(t)$, where $z_0(t)$ is a *defocusing* distance defined along $\mathbf{c}_2(t)$, f is the focal length of the focusing lens, and λ is the light wavelength in the medium. Note that, for the case of 2D curves described in the transverse x–y plane, $z_0(t) = 0$ holds.

In the case of a circle $x_0(t) + \mathrm{i}y_0(t) = \rho\exp(\mathrm{i}t)$, with ρ being a radius and $t \in [0, T = 2\pi]$, a ring vortex with topological charge m is obtained. In contrast to the well-known Gaussian vortex trap, this ring vortex is a *true* 3D trap able to confine particles far enough from the chamber walls and its topological charge can be increased without altering its radius [14,19]. Note that the radius of the ring trap in the focal plane (sample) is $R = \lambda \mathrm{f}/2\pi\rho$; see [19]. Further, the same value of ρ is used for generation of all the considered traps.

Figure 1(a) shows the phase distribution of a ring trap, with $R = 5$ μm and charge $m = 30$, and its corresponding 3D intensity profile generated by numerical focusing. The triangle-shaped trap (hypocycloid, given by $x_0(t) + \mathrm{i}y_0(t) = \rho(2\exp(\mathrm{i}t) + \exp(-\mathrm{i}2t)/2)$) with charge $m = 34$ displayed in Fig. 1(b) also exhibits high-intensity gradients. We underline that its phase gradient varies around the curve; see Fig. 1(b) and the zoom in Fig. 1(b1). In particular, the phase gradient increases when approaching the corner and then decreases after that. Therefore, it is expected that the motion (clockwise rotation in the considered examples) of the trapped particles speeds up when approaching the corner and then slows down after passing the trough and so on. This nonuniform phase gradient along the curve is due to its *intrinsic* phase, which is given as a function of the curvature changes. Indeed, a beam with non-zero charge m exhibits an *intrinsic* phase distribution described by the term $\exp(\mathrm{i}2\pi m S(t)/S(T))$ in Eq. (2). Specifically, the modulus of the phase gradient of the triangle-shaped beam $m = 34$ varies along the curve and has stationary points at each corner vertex (where it reaches a maximum value, SP1) and at the middle of each side (where it reaches a minimum value, SP2); see Fig. 1(c). This explains the phase gradient variations along the curve, as revealed by the phase pattern and the gradient vector field displayed in Figs. 1(b) and 1(b1). An understanding of the phase gradient behavior for noncircular curves is crucial in the study of the particle dynamics in freestyle traps.

Figure 2 displays the experimental results obtained for the trapping beams shaped in a ring (Fig. 2(a)), a triangle (Fig. 2(b)), and a square (Fig. 2(c)). The square-shaped beam corresponds to

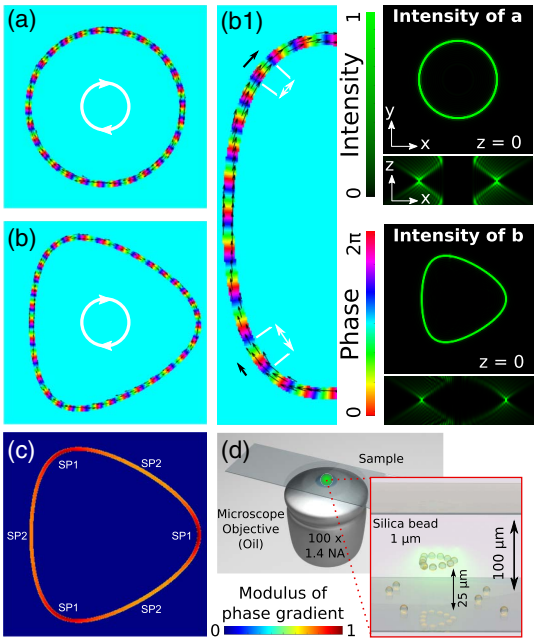

Fig. 1. Phase of the beam shaped in: (a) a ring and (b) a triangle with charges $m = 30$ and $m = 34$, respectively. Zoom inset (b1) corresponds to the phase shown in (b). Black arrows displayed in the phase represent its gradient vector field. (c) Modulus of the phase gradient for the triangle beam. SP indicates a stationary point where the modulus of phase gradient is maximum (SP1) or minimum (SP2). The 3D intensity profiles under focusing are shown for cases (a) and (b) as well. (d) sketch of the trapping configuration (inverted microscope).

an epicycloid curve given by $x_0(t) + iy_0(t) = \rho(3\exp(it) + 7\exp(-i3t)/20)$ and has $m = 34$. All the studied traps were created 25 μm deep in the sample, as sketched in Fig. 1(d). The trapped particles present uniform clockwise rotation in the case of the ring trap (see Visualization 1), while in the cases of the triangle (see also Visualization 1) and square (see Visualization 2), the particles speed up when approaching the corners, as previously discussed. To help the visualization of the beam–particle interaction, a time-lapse composition made by combining all the recorded frames into a single image is displayed for each case; see the right panel of Fig. 2. This allows one to observe the strong confinement of the particle flow along the curved beam. Indeed, all the particles fit tightly to the curve, which reveals the shape of the trapping beam. In the case of the square-shaped trap, a few particles eventually escape in the corners due to collisions between them; see time-lapse image (at bottom-right corner) in Fig. 2(c) and Visualization 2. As observed in Visualization 1 and Visualization 2, the flow of trapped particles can be switched in geometry (keeping almost all the particles) from the ring to the triangle and square in a few milliseconds just by changing the hologram $H(\mathbf{r}|\mathbf{c}_3)$ displayed in the SLM. This fact, together with the option to switch the motion direction ($m > 0$ clockwise and $m < 0$ anticlockwise) and to increase the rotation rate of the particles without altering the size and geometry of the beam, underline the versatility of the developed traps. To illustrate the switch of the motion direction and variable rotation rate of the particles, a ring trap with $m = \pm 15$ (rotation rate of 0.3 Hz) and $m = 30$ (rotation rate of 0.5 Hz), keeping the ring radius, are shown in Visualization 3. These results demonstrate that multiple small dielectric particles can be confined in different geometries and manipulated by variable phase gradient forces. Moreover, it is achieved far away from the chamber walls, thus avoiding unwanted hydrodynamic effects.

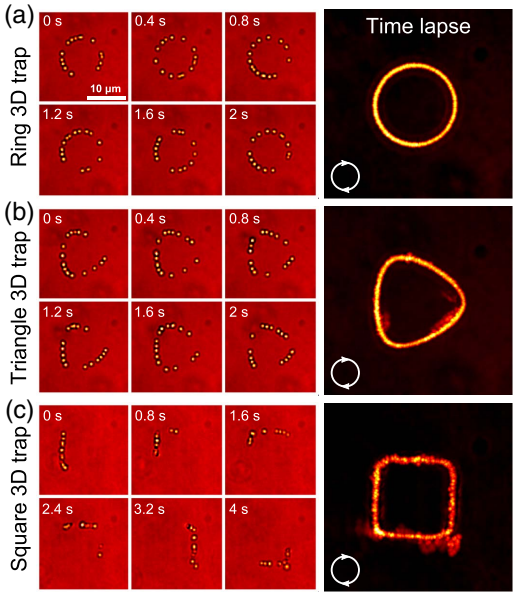

Fig. 2. Experimental results, Visualization 1 and Visualization 2. Laser traps shaped in (a) a ring with $R = 5$ μm; (b) a triangle; and (c) a square. A time-lapse image shows the flow of particles, revealing the beam shape. The ring (charge $m = 30$), triangle ($m = 34$), and square ($m = 34$) traps induce particle rotation with rates of 0.5, 0.25, and 0.14 Hz, respectively. The change of the vortex charge (phase gradient) does not alter the size or geometry of the trap; see Visualization 3.

More interesting particle dynamics can be studied by using 3D curved traps. In this case, the trapped particles move downstream and even upstream—against the light radiation pressure toward the laser source, as a tractor beam does [16,17]—thanks to the phase gradients. This is observed in different configurations: tilted ring trap (Fig. 3(a)) and the waved-ring traps displayed in Figs. 3(b) and 3(c); see also Visualization 4. Note that the image of the particle varies due to defocusing according to its 3D position with respect to the focal plane of the microscope objective lens, as observed in the time-lapse flow image. Interestingly, the rotation rate (range 0.4–0.5 Hz) is similar in the three traps considered, so the mean speed of the particles is preserved in spite of multiple upstream motions; see Fig. 3 and Visualization 4. Specifically, the particle motion in the upstream trajectory is slower than in the downstream one in which the particle speeds up, thus preserving the particle rotation rate in the trap. The phase gradient of the beam redirects part of the radiation pressure to create optical forces strong enough to move the particle upstream but also speeds up the particle in downstream motion; see [15] for further details. These results underline the important interplay between the light radiation pressure and phase gradients that drives the particle motion, whereas the HIGs maintain stable trapping along the 3D curve. Moreover, the latter examples illustrate how reconfigurable tractor beams can be created, controlled, and switched in real time; see Visualization 4.

By using the proposed technique, more complex particle flows extended in 3D curve geometries can be created. For example, in Fig. 4, a trap shaped by a spiral curve embedded in a toroidal surface is considered. The projection of this toroidal 3D trap has a starfish shape in the x–y plane, as revealed by the time-lapse flow image in Fig. 4. As in the previous examples, the particles are well confined and perform clockwise rotation following the curve. Nevertheless, while some particles move along the curve, others stay in quasi-stable equilibrium at the top vertices of the

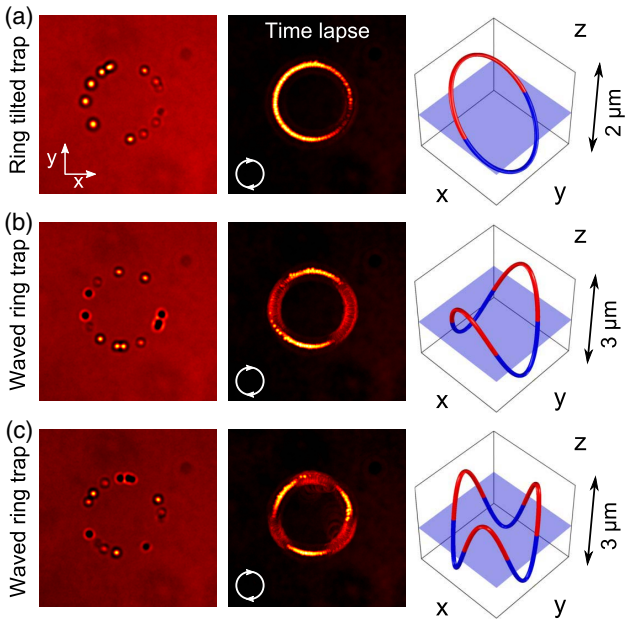

Fig. 3. Experimental results, Visualization 4. Laser 3D traps with radius $R = 5$ μm: (a) a ring tilted with $z(t) = 1$ μm $\sin(t)$; (b) a waved ring with $z(t) = 1.5$ μm $\sin(2t)$; and (c) a waved ring with $z(t) = 1.5$ μm $\sin(3t)$. The particle rotation rate is about 0.5 Hz.

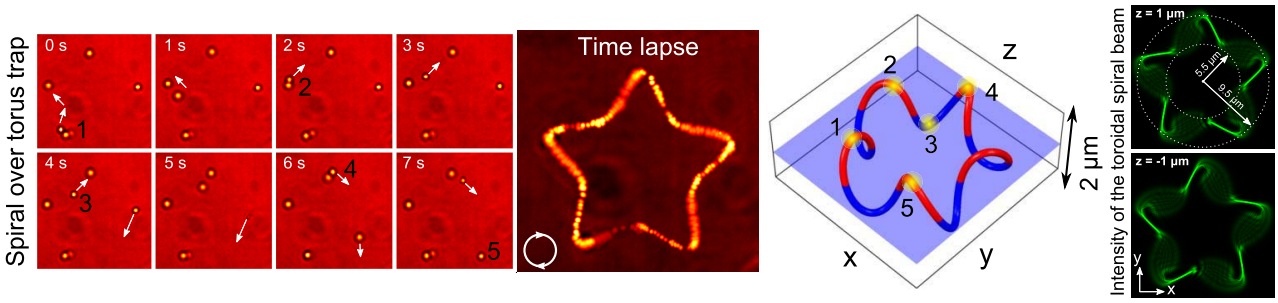

Fig. 4. Experimental results, Visualization 5, of the optically induced particle motion in a 3D toroidal-spiral laser trap. The time-lapse image shows the particle flow revealing a starfish shape, which is in good agreement with the shape of the trapping beam (right panel). Top and bottom corners of the 3D toroidal-spiral curve are plotted in red and blue, respectively.

curve (see Fig. 4), where the particle experiences a balance of forces. Visualization 5 shows a particle that starts at vertex 1 (see Fig. 4, time 0 s) and then reaches top vertex 2 after performing an up-down-stream motion in 2 s. At this point, it pushes another particle, releasing it from the quasi-stable equilibrium. This released particle goes toward vertices 3 and 4, performing another up-down-stream motion. Such *billard-like* behavior in the particle flow is extended along the entire trap. These results illustrate the role played by a freestyle trap as a tool to study interactions between particles.

In all the traps considered we have observed that a single trapped particle travels along the curve slower than in the case of multiple trapped particles. For example, in the ring trap, a single particle has a rotation rate of 0.2 Hz, whereas for multiple particles the rate increases up to 0.5 Hz (Visualization 1). This increase in the mean speed of the particles is caused by collective effects including hydrodynamic interactions [1,2]. Indeed, the trapped particles driven by the phase gradient force have the ability to push, and also to pull, neighboring particles due to hydrodynamic drafting [1], which is a characteristic of colloidal systems of particles moving in a viscous fluid (water).

Freestyle 3D laser traps provide important degrees of freedom in the design of optical forces that are able to confine and drive multiple particles, as required in numerous applications. For example, the 3D particle motion is well suited to construct a new generation of rotating colloidal motors that induce fluid flows in different geometries. These motors can be used for developing microfluidic tools or applied for rheological study of the immersion fluid. Freestyle traps also pave the way for designing Brownian ratchets [3] in which the external force switching the on and off states is the phase gradient force *prescribed* along the trap. Moreover, they allow for investigating important aspects of multiparticle dynamics induced by light and hydrodynamics interactions as well as optical binding effects [22]. The design of optical forces and their impact on the transport and organization of particles are also promising for micropattern generation.

Funding. Ministerio de Economía y Competitividad (Ministry of Economy and Competitiveness) (TEC2014-57394-P).

Acknowledgment. J. A .R. conceived the idea, developed the experimental setup, and carried out the experiments and programs. J. A. R. and T. A. analyzed the results and wrote the Letter.

REFERENCES

1. M. Reichert and H. Stark, J. Phys. **16**, S4085 (2004).
2. Y. Roichman, D. G. Grier, and G. Zaslavsky, Phys. Rev. E **75**, 020401 (2007).
3. A. Grimm and H. Stark, Soft Matter **7**, 3219 (2011).
4. A. Ashkin, *Optical Trapping and Manipulation of Neutral Particles Using Lasers: A Reprint Volume with Commentaries* (World Scientific, 2006).
5. H. He, M. E. J. Friese, N. R. Heckenberg, and H. Rubinsztein-Dunlop, Phys. Rev. Lett. **75**, 826 (1995).
6. E. G. Abramochkin and V. G. Volostnikov, Phys. Usp. **47**, 1177 (2004).
7. K. Ladavac and D. Grier, Opt. Express **12**, 1144 (2004).
8. A. Jesacher, S. Fürhapter, C. Maurer, S. Bernet, and M. Ritsch-Marte, Opt. Express **14**, 6342 (2006).
9. M. J. Padgett, J. E. Molloy, and D. Mcgloin, eds., *Optical Tweezers: Methods and Applications* (CRC Press, 2010).
10. G. Sinclair, P. Jordan, J. Courtial, M. Padgett, J. Cooper, and Z. Laczik, Opt. Express **12**, 5475 (2004).
11. S. Bianchi and R. D. Leonardo, Comput. Phys. Commun. **181**, 1444 (2010).
12. K. Volke-Sepulveda, V. Garcés-Chávez, S. Chávez-Cerda, J. Arlt, and K. Dholakia, J. Opt. B **4**, S82 (2002).
13. J. Baumgartl, M. Mazilu, and K. Dholakia, Nat. Photonics **2**, 675 (2008).
14. Y. Roichman and D. G. Grier, Proc. SPIE **6483**, 64830F (2007).
15. Y. Roichman, B. Sun, Y. Roichman, J. Amato-Grill, and D. G. Grier, Phys. Rev. Lett. **100**, 013602 (2008).
16. S. Sukhov and A. Dogariu, Opt. Lett. **35**, 3847 (2010).
17. S.-H. Lee, Y. Roichman, and D. G. Grier, Opt. Express **18**, 6988 (2010).
18. E. R. Shanblatt and D. G. Grier, Opt. Express **19**, 5833 (2011).
19. J. A. Rodrigo, T. Alieva, E. Abramochkin, and I. Castro, Opt. Express **21**, 20544 (2013).
20. S. N. S. Reihani and L. B. Oddershede, Opt. Lett. **32**, 1998 (2007).
21. M. Dienerowitz, G. Gibson, R. Bowman, and M. Padgett, Opt. Express **19**, 24589 (2011).
22. T. Cizmar, L. C. D. Romero, K. Dholakia, and D. L. Andrews, J. Phys. B **43**, 102001 (2010).